Spontaneous Oxidation of Ni Nanoclusters on MgO Monolayers Induced by Segregation of Interfacial Oxygen.

M. Smerieri[1‡], J. Pal[1,2‡], L. Savio[1], L. Vattuone[1,2], R. Ferrando[1,3], S. Tosoni[4], L. Giordano[4], G. Pacchioni[4], M. Rocca[1,2]*

1 IMEM-CNR, U.O.S. Genova, Via Dodecaneso 33, 16146 Genova, IT

2 Dipartimento di Fisica, Università di Genova, Via Dodecaneso 33, 16146 Genova, IT

3 Dipartimento di Chimica e Chimica Industriale, Università di Genova, Via Dodecaneso 31, 16146 Genova, IT

4 Dipartimento di Scienza dei Materiali, Università Milano Bicocca, via R. Cozzi 55, 20125 Milano, IT

Supporting Information

1. Experimental and theoretical methods.

The experiments were carried out in an ultra-high vacuum apparatus consisting of an analysis chamber, hosting a low temperature scanning tunneling microscope (LT-STM by Createc) and of a preparation chamber. The latter is equipped with a Knudsen cell and an O_2 doser for reactive Mg evaporation, with a quartz microbalance (QMB) for Mg flux measurements, with an e-beam evaporator (Focus EFM 3) mounting a high purity (99.99%) Ni rod, with an ion-gun plus gas inlet for sample cleaning and with a quadrupole mass spectrometer for residual gas analysis. Finally, a four degrees of freedom manipulator, coolable to liquid nitrogen temperature, allows precise positioning of the sample holder in front of the preparation tools and transfer inside the STM. The sample can be resistively heated up to 850 K.

The substrate is an Ag single crystal cut within 0.1° from the (100) plane. Before each experiment it was carefully cleaned by repeated cycles of sputtering and annealing to T=850 K till it showed clean and ordered terraces at the STM inspection. 0.7 ML (in monolayers of Ag(100)) MgO films were grown by reactive deposition at T=773 K, followed by post-annealing in O_2 atmosphere and slow cooling to T<450 K, as detailed in ref.[1]. Mg was evaporated from a crucible heated to 593 K, providing an evaporation rate of ~1 Å/min. The background pressure of O_2 during Mg evaporation was kept at $P_{O2}=1\cdot10^{-6}$ mbar but, since a doser placed at ~2 cm from the Ag(100) surface was employed, an effective pressure at least 5 times higher is expected[2]. The MgO film thickness was evaluated *a priori* from the Mg flux estimated through the quartz microbalance and *a posteriori* by inspection of STM images. The error assigned to the QMB is ±8%, while the Mg evaporation rate measured in different days under identical conditions is stable within 5%. Ni was deposited on the MgO/Ag(100) sample at T=200 K using an commercial e-beam evaporator (Focus EFM 3) and always in a background pressure better than $2\ 10^{-9}$ mbar. The Ni coverage, estimated a posteriori, from the analysis of the STM images, is ~0.2 ML.

Samples are cooled to T<150 K and inserted into the STM immediately after preparation.

STM images were recorded at liquid nitrogen temperature with a Pt/Ir tip cut in air under strain and then reshaped by controlled crashes into the surface, so that tunneling occurs effectively through an Ag tip. The images were acquired in constant current mode, with typical tunneling currents of ~0.2 nA and bias voltage -4.0 V<V<+4.0 V. The lateral size of the images and the orientation of the surface are determined from atomically resolved measurements of the clean Ag(100) surface; similarly, heights are calibrated on monatomic Ag steps. STM analysis was performed with the help of WSxM software[3].

DFT calculations on the periodic slab models are performed with version 5 of the Vienna Ab initio Simulation Package (VASP)[4]. The gradient corrected Perdue Burke Enzerhof (PBE) exchange-correlation functional[5] is employed. The basis set is expanded up to a kinetic energy cutoff of 400 eV. Core electrons are described by the projector-augmented-wave (PAW) method[6,7], whereas O(2s, 2p), Mg(3s, 2p), Ni(4s, 3p, 3d) and Ag(5s, 4d) electrons are treated explicitly. The long-range dispersion is evaluated following the semiempirical DFT+D2 approach, as originally proposed by Grimme[8]. The coefficients for Mg are modified to better describe adsorption on ionic MgO surfaces[9]. The 4x4 supercell for the simulations consists of 4 layers of Ag, where only the two upper layers are relaxed, and one layer of MgO. A Γ-centered mesh of 3x3x1 K-points is adopted. Spin polarization effects are considered.

2. Relative Stability of Ni_4 isomers on 1ML MgO/Ag(100)

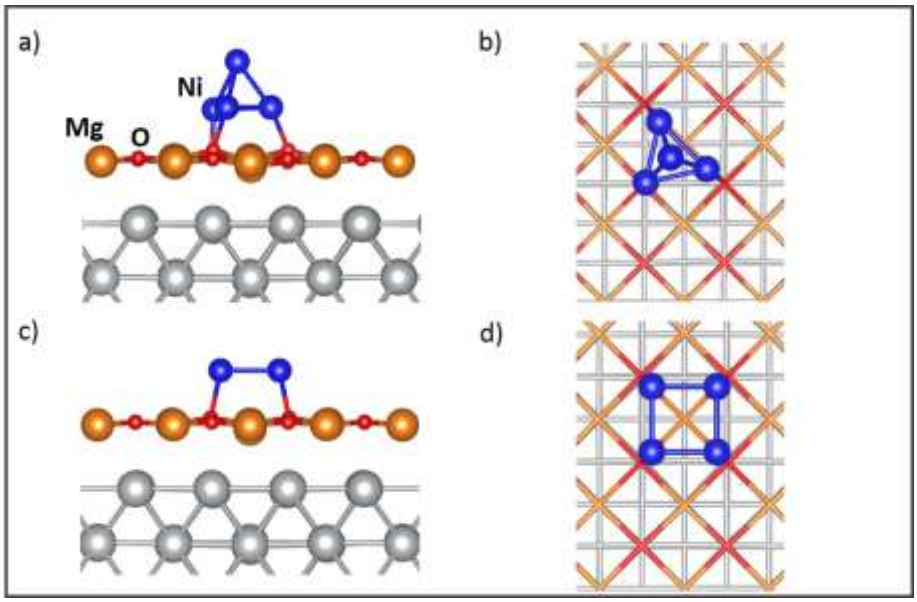

Figure S1. Ni_4 aggregates on MgO/Ag(100) as deduced from DFT calculations: a) side view and b) top view of the 3D structure; c) side view and d) top view of the 2D structure.

Table S1. Relative stability (and most stable structure) of 3D and 2D Ni_4 isomers as a function of O concentration at the MgO/Ag interface.

O_{int}	E(3D) – E(2D) (eV)
0%	-0.72 (3D)
25%	-0.47 (3D)
50%	+0.66 (2D)

3. Ni-Ni distances in Ni_yO_x aggregates

Table S2. Calculated and experimental Ni-Ni distances in Ni_yO_x aggregates on 1ML MgO/Ag.

Ni_n	Structure	Substrate Direction	R(Ni-Ni), calc [Å]	R(Ni-Ni), exp [Å]
4	Ni_4-3D/MgO/Ag	--	2.3-2.5	
	Ni_4-2D/MgO/Ag	<1-10> <001>	2.3 3.2	
	Ni_4O_5/MgO/Ag	<1-10> <001>	2.7 3.8	2.7 (1) 3.8 (2)
	Ni_4O/MgO/O_4/Ag	<1-10> <001>	2.3 3.2	
	Ni_4-3D/MgO/O_5/Ag	--	2.3-2.5	
5	Ni_5O_4/MgO/Ag	<0 0 1> <1-10>	2.9 2.2	
	Ni_5O_8/MgO/Ag	<0 0 1> <1-10>	3.8 2.7	4.4 (1) 3.2 (2)
	Ni_5O_{12}/MgO/Ag	<0 0 1> <1-10>	4.0 2.8	
6	Ni_6O_8/MgO/Ag	<1-10> <1-10>	2.7 2.6	2.7 (1) 3.0 (2)

The columns report the number of Ni atoms for each structure, the investigated system, the substrate direction along which the distance is measured, the calculated Ni-Ni distances and the corresponding experimental value, respectively. Notation (1) or (2) in the right column refers to the line scans marked in Figures 2 and 3 of the manuscript and S3 of the supporting material for T, P and H structures, respectively.

4. **Optimized structures and relative energies for Ni_4O_x clusters in the different configurations explored.**

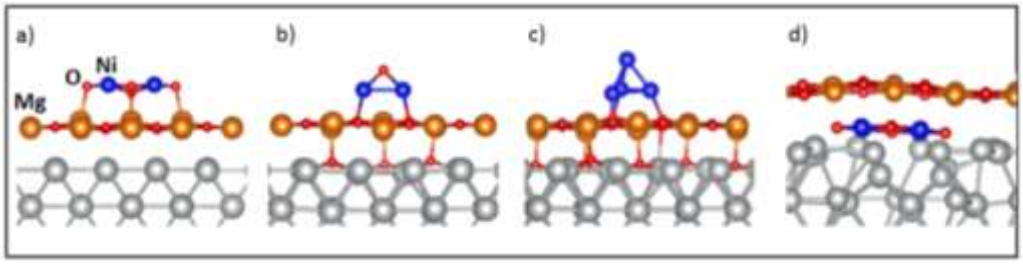

Figure S2. Side view of relaxed Ni_4O_x DFT structures. a) Ni_4O_5/MgO/Ag, b) Ni_4O/MgO/O_4/Ag, c) Ni_4/MgO/O_5/Ag and d) MgO/Ni_4O_5/Ag.

Table S3. Relative energies of Ni_4O_x structures.

Structure	E_{rel} (eV)
Ni_4O_5/MgO/Ag	0.0
Ni_4O/MgO/O_4/Ag	4.6
Ni_4/MgO/O_5/Ag	6.0
MgO/Ni_4O_5/Ag	0.7

5. Additional simulated Tersoff-Hamann images.

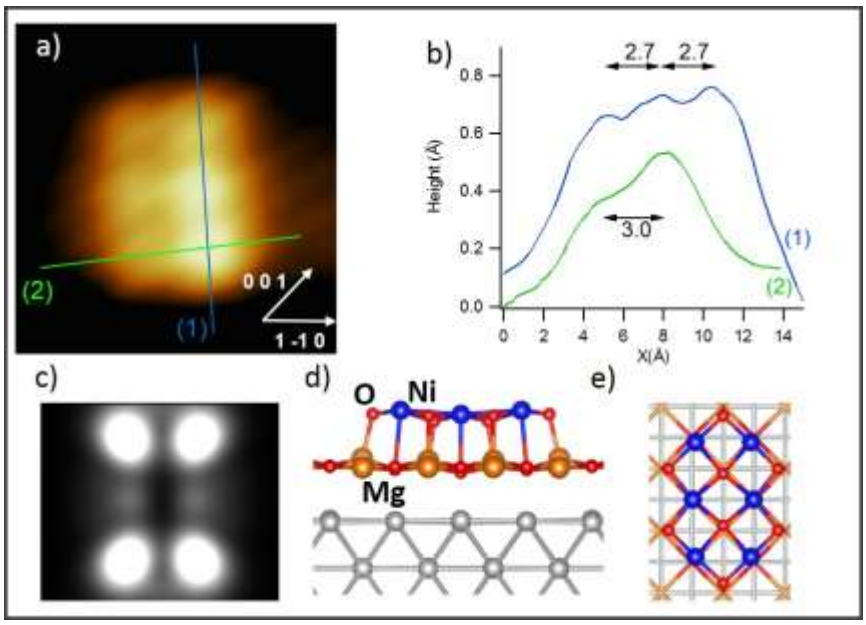

Figure S3. a) Atomically resolved STM image of a hexamer structure (15 x 16 $Å^2$, V=1.0 V, I=0.15 nA). The high symmetry directions of the substrate are marked. b) Line scans cut along the lines drawn in panel a) and showing the characteristic dimensions of the cluster. c) Tersoff-Hamann image of a Ni_6O_8 aggregate with bias V=+1.0 eV. The ISO level of charge density is set to 10^{-5} $|e|/Å^3$. d) and e) Most stable Ni_6O_8 aggregate on MgO/Ag(100) as deduced from DFT calculations (side and top view). This configuration was used as input for the simulated image.

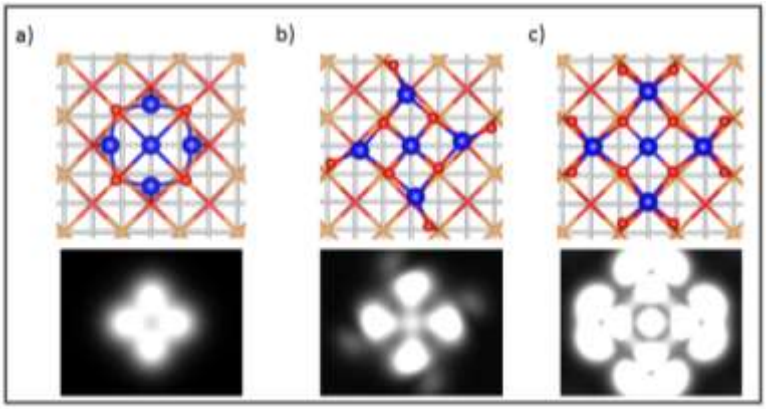

Figure S4. Top view (above) and Tersoff-Haman image with bias V=+1.0 eV of a) Ni_5O_4/MgO/Ag b) Ni_5O_8/MgO/Ag c) Ni_5O_{12}/MgO/Ag. The ISO level of charge density is set to 10^{-5} $|e|/Å^3$.

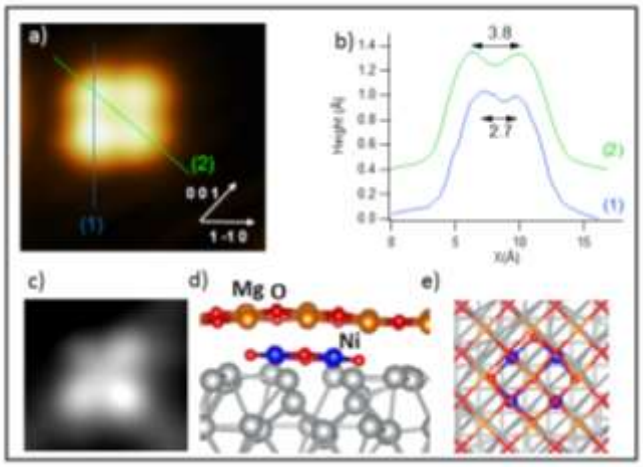

Figure S5. a) Atomically resolved STM images of a tetramer structure recorded at V=+1.0 V (18 x 18 $Å^2$, I=0.14 A). The high symmetry directions of the substrate are marked in the panel. b) Line scans cut along the lines drawn in panel a) and showing the characteristic dimensions of the cluster. c) Tersoff-Hamann images of $MgO/Ni_4O_5/Ag$ aggregate with bias V=+1.0 V. The ISO level of charge density is set to 10^{-5} $|e|/Å^3$. d) and e) $MgO/Ni_4O_5/Ag$ aggregate as deduced from DFT calculations (side and top view).

References

(1) Pal, J.; Smerieri, M.; Celasco, E.; Savio, L.; Vattuone, L.; Ferrando, R.; Tosoni, S.; Giordano, L.; Pacchioni, G.; Rocca, M., How Growing Conditions and Interfacial Oxygen Affect the Final Morphology of MgO/Ag(100) Films *Journal of Physical Chemistry C* **2014**, *118*, 26091.

(2) Henn, F. C.; Bussell, M. E.; Campbell, C. T., A SIMPLE MEANS FOR REPRODUCIBLY DOSING LOW VAPOR-PRESSURE AND OR REACTIVE GASES TO SURFACES IN ULTRAHIGH-VACUUM *Journal of Vacuum Science & Technology a-Vacuum Surfaces and Films* **1991**, *9*, 10.

(3) Horcas, I.; Fernandez, R.; Gomez-Rodriguez, J. M.; Colchero, J.; Gomez-Herrero, J.; Baro, A. M., WSXM: A software for scanning probe microscopy and a tool for nanotechnology *Review of Scientific Instruments* **2007**, *78*, 013705.

(4) Kresse, G.; Furthmuller, J., Efficiency of ab-initio total energy calculations for metals and semiconductors using a plane-wave basis set *Computational Materials Science* **1996**, *6*, 15.

(5) Perdew, J. P.; Burke, K.; Ernzerhof, M., Generalized gradient approximation made simple *Physical Review Letters* **1996**, *77*, 3865.

(6) Blochl, P. E., PROJECTOR AUGMENTED-WAVE METHOD *Physical Review B* **1994**, *50*, 17953.

(7) Kresse, G.; Joubert, D., From ultrasoft pseudopotentials to the projector augmented-wave method *Physical Review B* **1999**, *59*, 1758.

(8) Grimme, S., Semiempirical GGA-type density functional constructed with a long-range dispersion correction *Journal of Computational Chemistry* **2006**, *27*, 1787.

(9) Tosoni, S.; Sauer, J., Accurate quantum chemical energies for the interaction of hydrocarbons with oxide surfaces: CH_4/MgO(001) *Physical Chemistry Chemical Physics* **2010**, *12*, 14330.